Closed orbit change induced by nonzero dispersion rf cavities

Weiming Guo,* Katherine Harkay, and Michael Borland
Argonne National Laboratory, 9700 South Cass Avenue, Argonne, Illinois 60439, USA
(Received 5 July 2005; revised manuscript received 6 September 2005; published 18 November 2005)

The particle motion in storage rings is coupled between the longitudinal and the transverse planes in the presence of nonzero dispersion rf cavities. We found that the particle motion can be modeled separately with a redefined closed orbit. The closed orbit can be described by a Green's function, which was confirmed in the simulation and in the experiment. The pathlength is calculated from the redefined closed orbit, and we found that the longitudinal phase slip is related not only to the momentum, but also to the rf phase of the particle. The effect on the longitudinal motion becomes significant if the phase slip caused by the rf cavities is large or if the momentum compaction factor is small, such as in the lower alpha-*c* lattice which is intended to produce shorter bunches.

DOI: 10.1103/PhysRevE.72.056501 PACS number(s): 41.75.Lx, 29.27.Bd, 29.20.Dh, 29.20.Lq

I. INTRODUCTION

Synchrobetatron coupling (SBC) by nonzero dispersion cavities is a classical topic in accelerator physics. The phenomenon was first observed in the 6 GeV electron synchrotron NINA [1]. The rf cavity excites a betatron oscillation due to nonzero dispersion in the cavity, and the oscillation amplitude depends on the arrival time. On the other hand, the oscillation changes the path of the particle and affects the arrival time. Therefore, the particle motion is coupled in the horizontal and longitudinal planes. The beam becomes unstable when resonance conditions are met. Later it was found that beam-beam collision, cavity higher-order modes, and wakefields also induce SBC [2]. The SBC effect was believed to be innocuous if the beam motion is not on resonance. However, in the implementation of the low momentum compaction factor lattice, it was also found that SBC affects the longitudinal motion [3] and limits the minimum achievable bunch length [4]. Recently an application of nonzero dispersion rf cavities was proposed in a laser cooling scheme [5]. It becomes imperative to understand SBC at off-resonance but under extreme conditions like very low synchrotron frequency or very small longitudinal emittance.

Since the first observance of SBC, many models have been established. Piwinski and Wrulich [6] based their model on the closed orbit. They pointed out the closed orbit change induced by acceleration and modeled the betatron oscillation. The difficulty in their paper was the calculation of the longitudinal time delay caused by the betatron oscillation. In order to derive self-consistent treatment, Chao [7], Corsten and Hagedoorn [8], and Suzuki [9] developed a Hamiltonian perturbation theory that analyzed resonances with a so-called "SBC potential." Longitudinal and transverse nonlinear effects were added to the analysis by Baartman [10] and Lee [11]. The Hamiltonian method is good for resonance analysis; however, it does not give a satisfactory longitudinal phase shift.

In storage rings the betatron oscillation is much faster than the synchrotron oscillation. The SBC effect on the synchrotron motion is also slow compared to the betatron oscillation. We found that if we introduce a new closed orbit, the motion in both planes can be modeled separately. We treat the kick from a rf cavity as a dipole kick in the horizontal phase space. This dipole kick distorts the closed orbit like a dipole magnet and can be modeled by an analytical Green's function. This Green's function is verified both in the particle simulation and in the experiment. The longitudinal phase slip can therefore be calculated from the closed orbit. We further discuss the longitudinal motion with this phase slip and apply the result to two examples, in which the phase slip caused by the cavities is non-negligible. The layout of the paper is as follows. The equations of motion are derived in Sec. II, the closed orbit Green's function is derived in Sec. III, the simulation and experimental results are shown in Sec. IV, the longitudinal motion is discussed in Sec. V, and the conclusion is drawn in Sect. VI.

II. THE INHOMOGENEOUS HILL'S EQUATIONS

In this section the equations of synchrobetatron motion are derived from the Hamiltonian. The transverse motion of particles in a ring accelerator can be described by the following Hamiltonian [12]:

$$H = -p\left(1+\frac{x}{\rho}\right)\left(1-\frac{p_x^2+p_y^2}{p^2}\right)^{1/2} - eA_s, \tag{1}$$

where we use the curvilinear coordinate system (x,y,s), (x,p_x,y,p_y) are canonical conjugate coordinates, p is the total momentum, $\vec{A}=(A_x,A_y,A_s)$ is the vector potential, and ρ is the curvature of the reference particle path. Here we consider only the transverse magnetic fields, i.e., $A_x=A_y=0$.

In order to study the synchrobetatron coupling, p will be treated as a variable, namely,

$$p' = p_0\delta' = p_0\sum_i \frac{\Delta p_i}{p_0}\hat{\delta}(s-s_i), \tag{2}$$

where the prime is the derivative with respect to s, $\hat{\delta}$ is the Dirac delta function, $\Delta p_i/p_0$ is the fractional momentum

*Electronic mail: weguo@aps.anl.gov

kick, $\delta=(p-p_0)/p_0$, and p_0 is the momentum of the reference particle. We note that even though the accelerating field is not included explicitly in the Hamiltonian [Eq. (1)], Eq. (2) includes all the momentum changes along the path; therefore, the transverse motion is completely defined (up to first order).

From Hamilton's equation, one obtains the first-order horizontal equation of motion,

$$x'' + x'\delta' + K_\delta(s)x = \frac{\delta}{\rho}, \tag{3}$$

where $K_\delta(s)=1/\rho^2-K_1(s)-[2/\rho^2-K_1(s)]\delta$, $K_1(s)=B_1(s)/B_0\rho$ is the effective focusing strength, B_0 is the dipole field strength, and $B_1=\partial B_y/\partial x$ is the quadrupole gradient. Here only the dipole and quadrupole fields are considered.

The homogeneous equation of Eq. (3) is

$$x'' + x'\delta' + K_\delta x = 0. \tag{4}$$

The $x'\delta'$ term induces damping or growth of the betatron oscillation amplitude. Note that a similar term $(y'\delta')$ also appears in the equation of motion for y; therefore, synchrobetatron coupling affects both transverse planes. The change of the phase-space area is determined by the Wronskian. Let $x_1(s)$ and $x_2(s)$ be the linearly independent solutions of Eq. (4); then the Wronskian $W(x_1,x_2)(s)=W(x_1,x_2)(0)\exp[\delta(0)-\delta(s)]$. In storage rings $\delta(s)$ is a periodic function, and σ_δ is usually small ($\sim 10^{-3}$); therefore, the effect of the $x'\delta'$ term is also small. We will ignore it for now and discuss its impact later.

To find out the solution for the off-momentum particle, substitute $x(s)=x_\beta(s)+D(s)\delta$ into Eq. (3) (ignoring $x'\delta'$) and let the coefficients of δ vanish:

$$x_\beta'' + K_\delta x_\beta = -2D'\delta' - D\delta', \tag{5}$$

$$D'' + K_\delta D = \frac{1}{\rho}. \tag{6}$$

Equation (6) is the common dispersion equation, and Eq. (5) becomes an inhomogeneous equation due to the nonzero derivatives of δ.

The above inhomogeneous equations can be solved in vector space. Let $Z=(x,x')^T$, then Eq. (5) can be written as

$$\frac{d}{ds}Z = K_M Z - F_1\delta' - F_2\delta', \tag{7}$$

where

$$K_M = \begin{pmatrix} 0 & 1 \\ -K_\delta & 0 \end{pmatrix}, \tag{8}$$

and $F_1=(0,2D')^T$, $F_2=(0,D)^T$.

The homogeneous equation of Eq. (5) can be obtained by letting $\delta'=0$ and $\delta''=0$. Let $M(s)$ be the solution of the homogeneous equation of Eq. (5), i.e., $Z_h(s)=M(s)Z(0)$, with $Z(0)$ as the initial condition; then

$$M(s) = \exp\left(\int_0^s K_M\, ds\right), \tag{9}$$

and the solution of the inhomogeneous equation can be obtained from $M(s)$ by [13]

$$Z(s) = M(s)Z(0) - M(s)\int_0^s M^{-1}(s_1) \times [F_1(s_1)\delta'(s_1) + F_2(s_1)\delta''(s_1)]ds_1. \tag{10}$$

Equation (10) can be verified by direct substitution into Eq. (7).

Note $\delta''=(d/ds)\Sigma_i[\Delta p(s_i)/p_0]\hat{\delta}(s-s_i)$ is the derivative to the Dirac delta function. The F_2 term on the right-hand side of Eq. (10) becomes

$$M(s)\int_0^s M^{-1}(s_1)F_2(s_1)\delta''(s_1)ds_1 = -M(s)\int_0^s M^{-1}(s_1)F_3(s_1)\delta'(s_1)ds_1, \tag{11}$$

where $F_3=(-D,D')^T$ and the formulas $(M^{-1})'=-M^{-1}M'M^{-1}=-M^{-1}K_M$ have been used.

Combining Eqs. (11) and (10), one gets

$$Z(s) = M(s)Z(0) - M(s)\int_0^s M^{-1}(s_1)\vec{D}(s_1)\delta'(s_1)ds_1, \tag{12}$$

where $\vec{D}(s)=[D(s),D'(s)]^T$. Equation (12) means the momentum change gives the particle a transverse kick as follows:

$$\Delta x = -D\delta', \qquad \Delta x' = -D'\delta', \tag{13}$$

which clearly agree with the physical picture [6]. Note that the absence of the $x'\delta'$ term in Eq. (4) does not affect the results here because it only generates some higher-order terms. It is worth pointing out that the above equations can also be derived from the transformed Hamiltonian [14].

Similar to the inhomogeneous dispersion equation (6), Eq. (5) implies that the derivatives of the momentum also change the closed orbit. Let us examine δ' more closely before expanding Eq. (12). In electron storage rings, momentum kicks could be induced by the rf cavities, synchrotron radiation, and intrabeam scattering. Because synchrotron radiation is a random process, the kick is incoherent. The average energy of a bunch changes adiabatically during radiation energy loss, and the bunch moves gradually into its closed orbit. As a result, the bunch receives no coherent kicks from the energy loss of the individual particles. The momentum change due to collision has a similar effect. However, the momentum kick from the rf cavity is the same for all the particles with the same rf phase, and the average kick to a bunch is not

zero if the synchronous phase is not zero. Therefore, we expect coherent transverse effects induced by the rf cavity. From now on we define

$$\delta' = \sum_{n,i} \frac{\Delta p_i}{p_0} \hat{\delta}(s - s_i - nC), \tag{14}$$

where C is the circumference, $\hat{\delta}$ is the Dirac delta function, $\Delta p_i/p_0$ is the fractional momentum kick from the ith cavity, and n is the number of turns. We will first study the closed orbit change of a bunch, which resembles a single particle, then extend the result to a bunch slice while studying the longitudinal motion.

In order to calculate the closed orbit change given by Eq. (12), first one has to expand Eq. (9). It is difficult because δ is considered a variable in our model. However, one can use the solution of the reference particle ($\delta \equiv 0$) to obtain a perturbation solution. If $\delta \equiv 0$, $M(s)$ in Eq. (9) is just the transfer matrix of the reference particle. Mathematically, Eq. (12) can be expanded analytically with the transfer matrix; however, in the next section we solve it with another method that gives more physics insight. The method is essentially the same as expanding Eq. (12).

III. THE CLOSED ORBIT GREEN'S FUNCTION

We will solve for the closed orbit solution starting from Eq. (13). The horizontal kicks by a nonzero dispersion cavity are given by

$$\Delta x = -D(s_0)\frac{\Delta p(s_0)}{p_0} \quad \text{and} \quad \Delta x' = -D'(s_0)\frac{\Delta p(s_0)}{p_0}, \tag{15}$$

where s_0 is the cavity location and $\Delta p(s_0)/p_0$ is the fractional momentum kick. We note that the particle does not physically jump in x; the kick in space is because of the discontinuity of the reference closed orbit.

Because of this kick, the particle can no longer stay on the reference orbit, but rather has a betatron oscillation given by

$$x(s) = -\sqrt{\mathcal{H}(s_0)\beta(s)}\sin[\psi_{s,s_0} + \chi(s_0)]\frac{\Delta p(s_0)}{p_0},$$
$$x'(s) = \sqrt{\mathcal{H}(s_0)\gamma(s)}\sin[\psi_{s,s_0} + \chi(s_0) - \kappa(s)]\frac{\Delta p(s_0)}{p_0}, \tag{16}$$

where

$$\mathcal{H}(s_0) = \frac{1}{\beta(s_0)}\{D(s_0)^2 + (\alpha(s_0)D(s_0) + \beta(s_0)D'(s_0))^2\}, \tag{17}$$

$$\chi(s_0) = \tan^{-1}\frac{D(s_0)}{\alpha(s_0)D(s_0) + \beta(s_0)D'(s_0)}, \tag{18}$$

$$\kappa(s) = \tan^{-1}[1/\alpha(s)], \tag{19}$$

and $\alpha(s), \beta(s), \gamma(s)$ are the Courant-Snyder functions and $\psi_{s,s_0} = \psi(s) - \psi(s_0)$ is the phase advance from s_0 to s.

Due to the nonzero dispersion in the cavity, the total momentum gain is not purely in the s direction, but at an angle in the (x,s) plane. The effective fractional horizontal momentum gain is $dp_x/p_0 \sim x'(s_0)|_{x(s_0)=0} = \sqrt{\mathcal{H}(s_0)/\beta(s_0)}[\Delta p(s_0)/p_0]$. The momentum shifted into the horizontal direction is cancelled in the long run because the betatron oscillation tune is a noninteger. Therefore this process is dissipative. The lost fractional momentum is approximately $dp_z/p_0 \sim \frac{1}{2}|x'|^2_{x(s_0)=0} = [\mathcal{H}(s_0)/2\beta(s_0)][\Delta p(s_0)/p_0]^2$, which is a second-order term. The particle compensates this loss by moving to the right phase.

The oscillation is the same for a bunch slice, regardless of x and x' of the individual particles in the slice. This resembles the result of a dipole magnet kick. The difference is that the dipole magnet changes only x' but the rf cavity gives a vector kick; nonetheless, they are all dipole kicks in phase space.

If there are N cavities in a ring accelerator, the total horizontal displacement will be

$$x(s) = -\sqrt{\beta(s)}\sum_{i=1}^{N}\sqrt{\mathcal{H}(s_i)}\sin[\psi_{s,s_i} + \chi(s_i)]\frac{\Delta p(s_i)}{p_0}. \tag{20}$$

Summing over n turns, where $n = 0, 1, 2, \ldots$, and $n \ll 1/\nu_s$, with ν_s as the synchrotron tune, one gets

$$\begin{aligned} x(s) &= -\sqrt{\beta(s)}\sum_{i=1}^{N}\sqrt{\mathcal{H}(s_i)}\frac{\Delta p(s_i)}{p_0} \\ &\quad \times \mathrm{Im}[e^{i[\psi(s)-\psi(s_i)+\chi(s_i)]}(e^{i2\pi(n-1)\nu_x} + \cdots + 1)] \\ &= -\frac{\sqrt{\beta(s)}}{2\sin\pi\nu_x}\sum_{i=1}^{N}\sqrt{\mathcal{H}(s_i)}\frac{\Delta p(s_i)}{p_0} \\ &\quad \times [\cos\Psi(s,s_i) - \cos(\Psi(s,s_i) + 2n\pi\nu_x)], \end{aligned} \tag{21}$$

where

$$\Psi(s,s_i) = \psi(s) - \psi(s_i) + \chi(s_i) - \pi\nu_x, \tag{22}$$

ν_x is the horizontal tune, and $2\pi\nu_x > \psi(s) - \psi(s_i) \geq 0$. The first term in the bracket of Eq. (21) is independent of time; therefore, it represents the closed-orbit change. The second term is an oscillating term. One can define the closed-orbit Green's function of one cavity as follows:

$$G_{rf}(s,s') = -\frac{\sqrt{\beta(s)}}{2\sin\pi\nu_x}\sqrt{\mathcal{H}(s')}\cos\Psi(s,s'), \tag{23}$$

and the closed-orbit change due to all the cavities will be

$$x_{c.o.,rf}(s) = \sum_i G_{rf}(s,s_i)\frac{\Delta p(s_i)}{p_0}. \tag{24}$$

In Appendix A we give another method to derive this Green's function.

In order to study the properties of the terms in Eq. (21), we further define the lattice functions $\zeta(s)$ and $\xi(s)$ as

$$\zeta(s) = \frac{-\sqrt{\beta(s)}}{2\sin \pi\nu_x}\int_s^{s+C} ds' \frac{qE_{rf}(s')}{\hat{\beta}_0^2 E_0}\sqrt{\mathcal{H}(s')}\cos \Psi(s,s'), \tag{25}$$

$$\xi(s) = \frac{-\sqrt{\beta(s)}}{2\sin \pi\nu_x}\int_s^{s+C} ds' \frac{qE_{rf}(s')}{\hat{\beta}_0^2 E_0}\sqrt{\mathcal{H}(s')}\sin \Psi(s,s'), \tag{26}$$

where $E_{rf}(s')=dU(s')/ds'$ is the peak electric field strength in the rf cavities, and $\hat{\beta}_0$ and E_0 are the relativistic factor and the energy of the reference particle, respectively. Equation (21) becomes

$$x(s) = \zeta(s)\sin \phi - \sqrt{\zeta^2(s) + \xi^2(s)}$$

$$\sin \phi \cos[2n\pi\nu_x + \Upsilon(s)], \tag{27}$$

where $\Upsilon(s)=\tan^{-1} \xi(s)/\zeta(s)$, and $\zeta(s)\sin \phi$ is the closed-orbit change.

Differentiating Eqs. (25) and (26), one gets

$$\frac{d}{ds}\frac{\zeta(s)}{\sqrt{\beta(s)}} = -\frac{\xi(s)}{\beta^{3/2}(s)}, \tag{28}$$

$$\frac{d}{ds}\frac{\xi(s)}{\sqrt{\beta(s)}} = \frac{\zeta(s)}{\beta^{3/2}(s)}. \tag{29}$$

Consequently,

$$\frac{d}{ds}\left[\left(\frac{\zeta(s)}{\sqrt{\beta(s)}}\right)^2 + \left(\frac{\xi(s)}{\sqrt{\beta(s)}}\right)^2\right] = 0, \tag{30}$$

$$\frac{d}{ds}\Upsilon(s) = \frac{1}{\beta(s)}. \tag{31}$$

Therefore $\sqrt{\zeta^2(s)+\xi^2(s)}=\sqrt{C_{rf}(s)\beta(s)}$, where $C_{rf}(s)$ is a constant between two rf cavities, and $\Upsilon(s)$ is the betatron phase advance. Both $C_{rf}(s)$ and $\Upsilon(s)$ are discontinuous at the rf cavity locations because the rf cavities are the perturbation sources. Note that $\Psi(s,s_i)$, defined in Eq. (22), is not continuous at these locations either. Nonetheless the closed orbit $x_{c.o.}(s)=D(s)\delta+\zeta(s)\sin \phi$ is continuous.

The second term in Eq. (27) is a definite betatron oscillation term. It damps down after the bunch finds the closed orbit. Because of the $\zeta \sin \phi$ term, the transverse beam size is related to the longitudinal bunch length and is given by

$$\sigma_x^2 = \beta_x\epsilon_x + D^2\sigma_\delta^2 + \zeta^2 \cos^2 \phi_s\sigma_\phi^2. \tag{32}$$

The beam size increases because of the kicks from the rf cavities. As a comparison, the transverse emittance also contributes to the bunch length due to synchrobetatron coupling; refer to [4] for details.

Take the Advanced Photon Source (APS) storage ring as an example. There are 16 cavities distributed in four straight sections with four cavities each. The lattice functions are almost constant in all straight sections, particularly $\beta_x \sim 20$ m, $\gamma_x \sim 0.05$ m^{-1}, and $\mathcal{H} \sim 0.0015$ m. In each cavity the momentum change is $\Delta p/p \sim 5\times 10^{-5}$; from Eq. (16) one gets a betatron oscillation amplitude of 8 μm or so. The betatron phase advance between the four cavities in one straight section is small, and the phase advance in one sector is close to 2π. Therefore, from Eq. (24) it follows that the betatron oscillation caused by all cavities almost adds up coherently. Figure 1 shows the calculated closed orbit change under the current operation conditions. The maximum amplitude is about 0.1 mm, which is small compared to the dispersion function, e.g., $D_{x,max} \sim 0.2$ m. This justifies our modeling approach, which is based on the dispersion effect. As a reference, the $C_{rf}(s)$ function is plotted in Fig. 2. The maximum value of $C_{rf}(s)$ is about 1 nm. Because both ζ and σ_ϕ are small, the beam size contribution of the third term in Eq. (32) is very small.

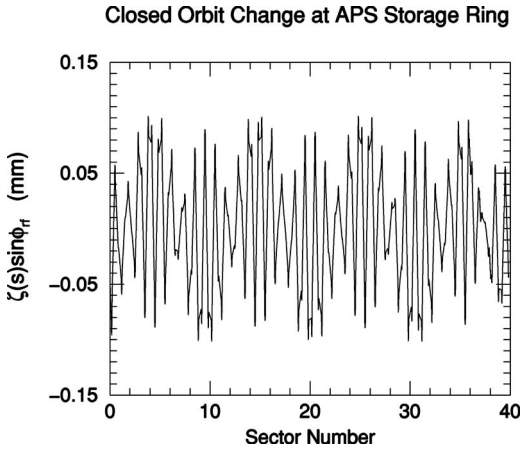

FIG. 1. The calculated closed-orbit change at the APS storage ring due to rf cavities. The parameters are as follows: total rf voltage U_{rf}=9.2 MV; synchronous phase ϕ_{rf}=144.36°.

IV. PARTICLE SIMULATION AND EXPERIMENTAL VERIFICATION

A. Orbit change outside the rf zone

The closed-orbit change can be measured by varying the rf voltage distribution at a constant rf frequency. The con-

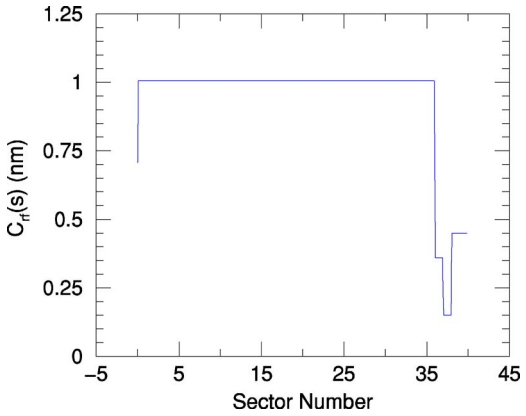

FIG. 2. (Color online) The $C_{rf}(s)$ function of the APS storage ring. It changes value only in the straight sections of sectors 36, 37, 38, and 40, where rf cavities are placed.

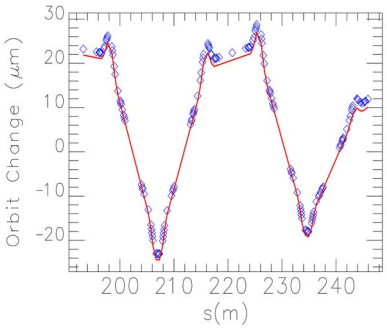

FIG. 3. (Color online) The comparison of the orbit change between the simulation (the diamonds) and the prediction (the solid line) in part of the ring outside the rf zone. The agreement is similar in the part outside the rf zone.

stant rf frequency ensures constant beam energy; therefore, the dispersion effect is excluded. In the APS storage ring the rf cavities are placed in sectors 36, 37, 38, and 40. Outside the rf zone the bunch energy is the same if the rf frequency is not changed; however, inside the rf zone the beam energies are different when the voltage distribution is varied. First we discuss the changes outside the rf zone.

The rf cavities at the APS are powered by two klystrons. The power from each klystron can be adjusted by ±20%, which results in about a 20 micron maximum closed-orbit change. This is well within the time-averaged resolution of the APS beam position monitor (BPM) system, which is approximately one micron.

Particle simulations were first carried out with code ELEGANT [15]. One particle was tracked for 12 000 turns using the APS lattice. Both radiation energy loss and quantum excitation were included in the tracking. Since the horizontal damping time is about 2600 turns, the trajectory of the particle on the final turn is the closed orbit. Two simulation runs were performed. In the first run the voltage was 0.5625 MV per cavity with a total gap voltage of 9 MV, which simulates the normal operating condition. In the second run the first eight cavities (in sectors 36 and 37) were set to 0.375 MV while the voltages of the other eight cavities (in sectors 38 and 40) were 0.75 MV. The closed-orbit difference between two simulations is shown in Fig. 3. The theory is in excellent agreement with the simulation result.

In the experiment, the voltages in the first eight cavities were changed in ten steps from 0.625 to 0.425 MV, meanwhile the reverse was done for the second eight cavities. The total voltage was kept constant. For each step the closed orbit was recorded by BPMs and averaged for one second. Even though the power coupling in each cavity was slightly different, the voltage step size was almost equal for all 16 cavities, except the sign.

From Eq. (24) the closed-orbit change between the two setups will be

$$\Delta x_{c.o.,rf}(s) = \sum_i G_{rf}(s,s_i)\left(\frac{\Delta p_2(s_i)}{p_0} - \frac{\Delta p_1(s_i)}{p_0}\right)$$

$$= \frac{\Delta V \sin\phi_s}{E_0}\sum_i \pm w_i G_{rf}(s,s_i), \qquad (33)$$

where 1 and 2 stand for the two setups, ΔV is the voltage change in units of MV, E_0 is the energy of the particle in units of MeV, and w_i close to 1 is the coupling factor. Therefore, at one location the closed-orbit change is proportional to the voltage change in our experiment. Be aware that Eq. (33) is true only when the total voltage is kept constant and the voltage step size is constant for one cavity. Figure 4 shows an example of the closed-orbit changes at one BPM, and they did appear to be a linear function of ΔV. The slopes obtained from the fitting are compared with theory in Fig. 5; again they are in good agreement.

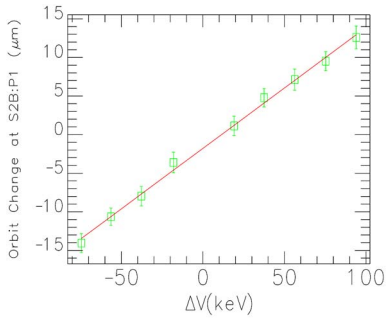

FIG. 4. (Color online) The measured closed-orbit change at BPM S2B:P1 while ΔV is varied. The squares indicate the experimental data and the line is the linear fit. The total gap voltage was kept constant and the voltage step size was fixed for each cavity. The slope obtained by fitting is discussed in Fig. 5.

Orbit change inside the rf zone

The particle in the APS storage ring loses 5.4 MeV energy each turn due to synchrotron radiation, and the same amount of energy is replenished by the rf cavities. The rf zone is from sector 36 to sector 40 in the 40-sector ring. If the beam energy at the entrance of the first cavity is E_A, then between cavity k and $k+1$,

$$E(s) = E_A + \sum_{i=1}^{k} U_i \sin\phi_s - \Delta E_r(s), \qquad (34)$$

where U_i is the peak voltage in the ith cavity, and $\Delta E_r(s)$ is the radiation energy loss from the first cavity to s.

When the voltage distribution is changed, the energy difference at the same location is given by

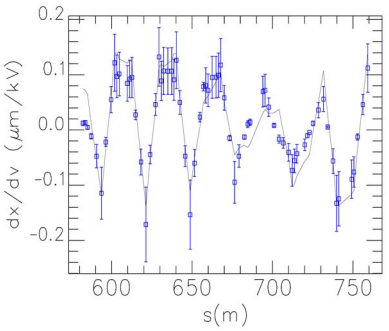

FIG. 5. (Color online) The comparison of the slopes of $dx_{c.o.}/d\Delta V$ outside the rf zone. The squares were obtained from the experiment and the line is from the calculation.

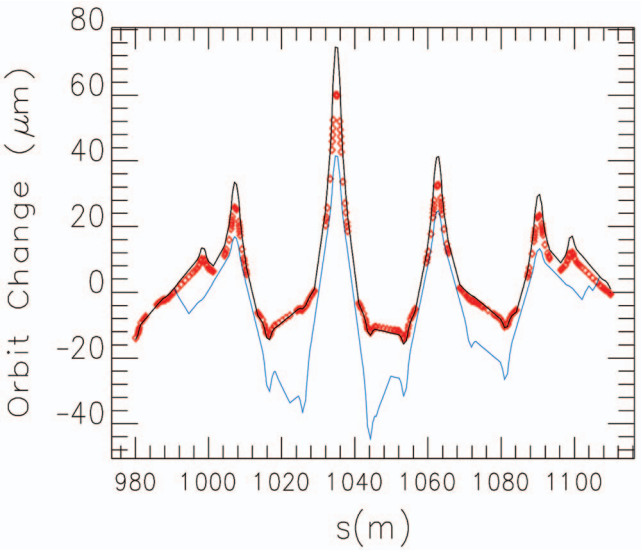

FIG. 6. (Color) The closed-orbit change inside the rf zone. The red diamonds are from the simulation, the blue line is the calculated $\zeta(s)\sin\phi_{rf}$ difference only, and the black line is calculated from Eq. (36), including the dispersion effect.

$$\Delta E(s) = \sum_{i=1}^{k} (U_{i,2} - U_{i,1})\sin\phi_s, \tag{35}$$

where 1 and 2 stand for the initial and final distributions.

Therefore, the total closed orbit change inside the rf zone is also related to the dispersion:

$$\Delta x_{c.o.} = \zeta_2(s)\sin\phi_s - \zeta_1(s)\sin\phi_s + D(s)\frac{\Delta E(s)}{\hat{\beta}_0^2 E_0}. \tag{36}$$

Figure 6 shows the simulated closed-orbit change inside the rf zone. Both the simulation and the experiment parameters are the same as those in Sec. IV A. When the dispersion effect is included, the theory agrees very well with the simulation. The experimental result is shown in Fig. 7, and the agreement is reasonable.

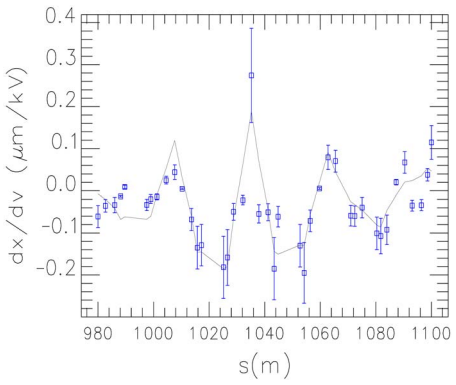

FIG. 7. (Color online) The slope of $dx_{c.o.}/d\Delta V$ inside the rf zone. The squares with an error bar are obtained from the experiment. The dispersion term was subtracted from the original orbit data change, and the slope is obtained by fitting the difference with ΔV. The line is the slope from the calculation.

V. THE RELATED LONGITUDINAL MOTION

So far the closed-orbit change in the transverse direction has been examined, and we are ready to study the longitudinal motion. The energy gain of a particle from the rf cavity in one passage is given by

$$\frac{\Delta p_z}{p_0} = \frac{qU\sin\phi}{\hat{\beta}\hat{\beta}_0 E_0} \approx \frac{qU(r)\sin\phi}{\hat{\beta}_0^2 E_0}, \tag{37}$$

where $\hat{\beta}_0$ and E_0 are the relativistic factor and the energy of the reference particle, q and $\hat{\beta}$ are the charge and relativistic factor of the study particle, $U(r)$ is the peak voltage of the rf cavity, and $r=\sqrt{x^2+y^2}$. For the pillbox cavity working at the TM_{010} mode, $k_r \approx 2.405/r_c$, with r_c as the radius of the cavity, and $U(r)$ is proportional to the zeroth-order Bessel function of r; therefore, $U(r) \approx U_0(1-1/4k_r^2x^2)$.

The fractional momentum difference from the synchronous particle in one turn will be

$$\frac{d\delta}{d\theta} = \sum_{s}^{s+C} \frac{q}{2\pi\hat{\beta}_0^2 E_0}[U(s,r)\sin\phi - U(s,0)\sin\phi_s], \tag{38}$$

where $\delta=(p-p_0)/p_0$, $\Delta\phi=\phi-\phi_s$, $\theta=2\pi n$ ($n=1,2,3,\ldots$, is the orbital angle).

The closed orbit for a particle with fractional momentum δ and rf phase ϕ can be written as

$$x_{c.o.}(s) = x_{c.o.,0}(s) + D(s)\delta + \zeta(s)\cos\phi_s\,\Delta\phi + \lambda_{\delta,2}(s)\delta^2 + \lambda_{\phi,2}(s)\Delta\phi^2 + \lambda_{\phi,\delta}(s)\Delta\phi\,\delta + \mathcal{O}(3), \tag{39}$$

where $x_{c.o.,0}(s)$ is the closed orbit distortion, which can be assumed to be zero. λ factors can be determined by tracking or measurement since they are also related to the sextupole and all the higher-order multipole fields [16].

From Eq. (39), Eq. (38) becomes

$$\frac{d\delta}{d\theta} = \frac{qU_T\cos\phi_s}{2\pi\hat{\beta}_0^2 E_0}\Delta\phi + \kappa_{\phi,2}\Delta\phi^2 + \kappa_{\phi,\delta}\Delta\phi\,\delta + \kappa_{\delta,2}\delta^2 + \mathcal{O}(3), \tag{40}$$

where $U_T=\Sigma_s^{s+C}U(s)$ is the total gap voltage, the κ factors are defined as $\kappa_{\phi,2}=\langle\zeta^2\cos^2\phi_s - 1/2k_r^{-2}\rangle$, $\kappa_{\delta,2}=\langle D^2\rangle$, $\kappa_{\phi,\delta}=\langle 2D\zeta\cos\phi_s\rangle$, and $\langle f(s)\rangle = (8\pi\hat{\beta}_0^2E_0)^{-1}\Sigma_s^{s+C}qU(s)\sin\phi_s k_r^2 f(s)$.

From Eq. (39) the pathlength difference from the synchronous particle is

$$\frac{\Delta l}{l} = \alpha_{\phi,1}\cos\phi_s\,\Delta\phi + \alpha_{\delta,1}\delta + \alpha_{\phi,\delta}\Delta\phi\,\delta + \alpha_{\delta,2}\delta^2 + \alpha_{\phi,2}\Delta\phi^2 + \mathcal{O}(3). \tag{41}$$

And the alpha factors are defined as $\alpha_{\delta,1}=\langle AD\rangle$,

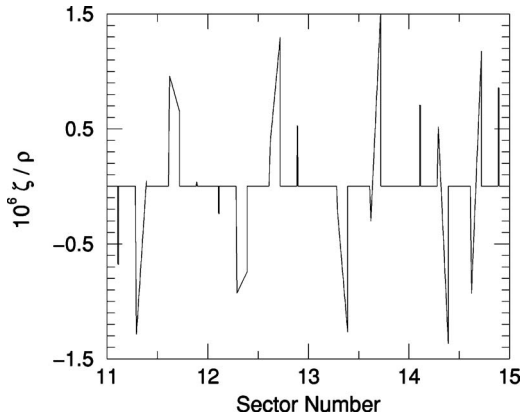

FIG. 8. $\zeta(s)/\rho(s)$ in part of the ring.

$\alpha_{\phi,1}=\langle A\zeta\cos\phi_s\rangle$, $\alpha_{\phi,\delta}=\langle A\lambda_{\phi,\delta}+A^2D\zeta\cos\phi_s+D'\zeta'\cos\phi_s\rangle$, $\alpha_{\delta,2}=\langle\frac{1}{2}A^2D^2+A\lambda_{\delta,2}+\frac{1}{2}D'^2\rangle$, $\alpha_{\phi,2}=\langle 1/2A^2\zeta^2\cos^2\phi_s+A\lambda_{\phi,2}+\frac{1}{2}\zeta'^2\cos^2\phi_s\rangle$, where $\langle f(s)\rangle=\frac{1}{C}\int_s^{s+C}f(s)ds$, $C=C_0(1+\alpha_\phi\sin\phi_s)$ is the closed-orbit length of the reference particle, $A(s)=1/\rho(s)$, and $\rho(s)$ is the radius of the orbit. Note that $\alpha_{\delta,1}$ is the usual first-order momentum compaction factor, and $\alpha_{\phi,1}$ is the first-order phase slip factor caused by the cavity-induced closed-orbit change. In practice, the alpha factors can be measured [17].

Hence, the total phase change per turn can be expressed as

$$\frac{d\Delta\phi}{d\theta}=h\eta_{\phi,1}\cos\phi_s\,\Delta\phi+h\eta_{\delta,1}\delta+h\eta_{\phi,\delta}\Delta\phi\delta+h\eta_{\delta,2}\delta^2+h\eta_{\phi,2}\,\Delta\phi^2+\mathcal{O}(3), \tag{42}$$

where h is the rf harmonic number, $\eta_{\delta,1}=\alpha_{\delta,1}-1/\hat{\gamma}_0^2$, $\eta_{\phi,1}=\alpha_{\phi,1}$, $\eta_{\phi,\delta}=\alpha_{\phi,\delta}-\alpha_{\phi,1}/\hat{\gamma}_0^2$, $\eta_{\delta,2}=\alpha_{\delta,2}+(1+\hat{\beta}_0^2/2-\alpha_{\delta,1})/\hat{\gamma}_0^2$, $\eta_{\phi,2}=\alpha_{\phi,2}$, and $\hat{\beta}_0$, $\hat{\gamma}_0$ are the relativistic factors.

Equations (40) and (42) define the longitudinal motion. For APS, $\eta_{\phi,1}=3.9\times10^{-11}$, which is much less than $\eta_{\delta,1}=2.8\times10^{-4}$; therefore, $\eta_{\phi,1}$ does not affect the longitudinal beam motion at APS. However, there are circumstances where $\eta_{\phi,1}$ cannot be ignored. One is in a specially designed lattice where $\eta_{\phi,1}$ is large; the other is when the first-order momentum compaction factor is small, e.g., in the lower alpha-c lattice. These two cases are discussed in the following sections.

A. Longitudinal damping lattice

$\alpha_{\phi,1}$ can be made large in a specially designed lattice. The integrand in the definition of $\alpha_{\phi,1}$ can be examined more closely. Figure 8 shows $\zeta(s)/\rho(s)$ in several sectors of the APS. In the dipole magnets $\zeta(s)/\rho(s)$ is of the order of 10^{-6}, and the total integral is small because $\zeta(s)$ changes sign frequently along the ring. Since rf cavities resemble dipole magnets, they can be arranged to form an orbit bump. Inside the bump, $\zeta(s)/\rho(s)$ can be kept the same sign; therefore, α_ϕ will be of the same order as $[\zeta(s)/\rho(s)][\Delta l/C]$. There are other methods to increase α_ϕ, too, like intentionally tilting the rf cavities. A horizontally tilted cavity gives the particle a phase ϕ related transverse kick, which has a similar effect as the nonzero dispersion cavity. In Appendix B the equilibrium angle in the cavities is discussed.

When $\alpha_{\phi,1}$ cannot be ignored, keeping only the leading terms in Eqs. (40) and (42) and rewritting them in $\Xi=(\Delta\phi,\delta)^T$ phase space, one gets

$$\Xi'=\begin{pmatrix} h\eta_{\phi,1}\cos\phi_s & h\eta_{\delta,1} \\ \dfrac{qU_T}{2\pi\hat{\beta}_0^2E_0}\cos\phi_s & 0\end{pmatrix}\Xi, \tag{43}$$

where the prime is the first derivative with respect to θ.

Solving the eigenvalue equation, one obtains the eigenfrequencies

$$\Omega_\pm=\iota\pm\sqrt{\iota^2-\nu_s^2}, \tag{44}$$

where

$$\iota=\tfrac{1}{2}h\eta_{\phi,1}\cos\phi_s,$$

and

$$\nu_s=\sqrt{-h\eta_{\delta,1}qU_T\cos\phi_s/2\pi\hat{\beta}_0^2E_0}.$$

Therefore, the longitudinal tune is affected by $\alpha_{\phi,1}$. We note that $\alpha_{\phi,1}$ is different for individual particles because of the incoherent momentum kicks induced by synchrotron radiation and intrabeam scattering. Consequently, the incoherent longitudinal tune will be different.

Usually $\iota\ll\nu_s$, and the solution to Eq. (43) is

$$\Delta\phi=-\frac{h\alpha_{\delta,1}}{\nu_s}\delta_0e^{\iota\theta}\left(\frac{\iota}{\nu_s}\sin\nu_s(\theta+\theta_0)+\cos\nu_s(\theta+\theta_0)\right),$$
$$\delta=\delta_0e^{\iota\theta}\sin\nu_s(\theta+\theta_0), \tag{45}$$

where δ_0 and θ_0 are determined by the initial conditions.

The stable conditions are

$$\eta_{\delta,1}\cos\phi_s<0\quad\text{and}\quad\eta_{\phi,1}\cos\phi_s<0. \tag{46}$$

The first inequality is the usual stable condition for synchrotron motion. The second inequality means $\eta_{\phi,1}$ must be negative below transition and positive above transition. The longitudinal phase space shrinks when the above conditions are met, meanwhile the transverse emittances grow according to Eq. (4). The total phase space volume is not preserved because of the dissipative transverse kicks from the rf cavities. This effect is very small, and it could be overwhelmed by many other factors. We are still looking for evidence that supports this conclusion.

B. Lower alpha-c lattice

The lower alpha-c lattice has been installed in several electron storage rings recently [3,18]. The electron bunch length is usually of the order of a few picoseconds due to the lowered momentum compaction factor. The lattice is used for coherent synchrotron radiation generation and time-resolved x-ray photography. The bunch length, however,

saturates when momentum compaction factor goes below a threshold value. Besides that, there are some interesting experimental phenomena that remain to be understood [18]. Proper modeling of the longitudinal motion seems to be crucial. In the lower alpha-c lattice, the dispersion function is significantly increased in the straight sections where the rf cavities are located; hence, $\eta_{\phi,1}$ is larger than that of the normal lattice. On the other hand, $\eta_{\delta,1}$ is minimized by orders of magnitude. Therefore, $\eta_{\phi,1}$ must be taken into account in the modeling of the longitudinal motion. The higher-order η_ϕ terms can be ignored because they are likely to be small. Therefore, the longitudinal motion can be described by

$$\frac{d\delta}{d\theta} = \frac{qU_T \cos\phi_s}{2\pi\hat{\beta}_0^2 E_0}\Delta\phi + \kappa_{\phi,2}\,\Delta\phi^2 + \kappa_{\phi,\delta}\Delta\phi\,\delta + \kappa_{\delta,2}\delta^2,$$

$$\frac{d\Delta\phi}{d\theta} = h\eta_{\phi,1}\cos\phi_s\Delta\phi + h\eta_{\delta,1}\delta + h\eta_{\delta,3}\delta^3, \qquad (47)$$

where $\eta_{\delta,2}$ is zero because of the symmetry [17]. Ignoring the κ terms and differentiating the first equation, one gets the equation for δ,

$$\delta'' = h\eta_{\phi,1}\cos\phi_s\delta' - \nu_{s,1}^2\delta - \nu_{s,3}^2\delta^3, \qquad (48)$$

where $\nu_{s,i} = \sqrt{-(h\eta_{\delta,i}qU_T\cos\phi_s)/(2\pi\hat{\beta}_0^2E_0)}$. For the electron storage ring BESSY's lower alpha-c lattice, $\nu_{s,3}^2\sigma_\delta^2 \ll \nu_{s,1}^2$, so we can treat the δ^3 term as a perturbation. In this case the stability conditions for Eq. (48) are the same as those in Eqs. (46). In BESSY's lower alpha-c operation, it was found that the total momentum compaction factor had to be less than zero to ensure a sufficiently large longitudinal bucket. This could be related to the $\eta_{\phi,1}$ factor. The complete solution of Eq. (47) is beyond the scope of this paper. It is worth mentioning that the η_ϕ terms should also be considered in the modeling of the transition energy crossing.

VI. CONCLUSION

The synchrobetatron coupling caused by nonzero dispersion rf cavities is a classical topic in accelerator physics. The current theory focuses mostly on the resonance. We have studied synchrobetatron coupling effect at off-resonance. Starting from the Hamiltonian, we found that the cavity can approximately be described by an equivalent dipole kicker; therefore, it changes only the closed orbit to the first order. The change can be described by an analytical Green's function, which was verified in the simulation and in the experiment. The longitudinal phase slip is calculated from the redefined closed orbit. We found that the phase slip is therefore related to both the momentum and the longitudinal position of the particle. The synchrobetatron coupling effect on the longitudinal motion becomes non-negligible if the phase slip induced by the cavities is big or if the momentum compaction factor is small. Longitudinal beam dynamics is discussed in both cases. We believe it has a significant effect on the lower alpha-c lattice.

ACKNOWLEDGMENTS

The authors wish to thank Louis Emery and Vadim Sajaev for offering information on machine setups, and Chun-xi Wang for the insightful discussions. This work was supported by the U.S. Department of Energy, Office of Basic Energy Sciences, under Contract No. W-31-109-ENG-38.

APPENDIX A: THE GREEN'S FUNCTION FOR A DIPOLE KICK IN PHASE SPACE

Consider a dipole kick in horizontal phase space at location $s=s_0$ in an otherwise ideal storage ring with

$$\Delta x = A, \quad \Delta x' = B. \qquad (A1)$$

However, the closed-orbit condition requires

$$\begin{pmatrix} x_0 - A \\ x_0' - B \end{pmatrix} = M_T \begin{pmatrix} x_0 \\ x_0' \end{pmatrix}, \qquad (A2)$$

where

$$M_T = \begin{pmatrix} \cos 2\pi\nu_x + \alpha(s_0)\sin 2\pi\nu_x & \beta(s_0)\sin 2\pi\nu_x \\ -\gamma(s_0)\sin 2\pi\nu_x & \cos 2\pi\nu_x - \alpha(s_0)\sin 2\pi\nu_x \end{pmatrix} \qquad (A3)$$

is the one-turn transfer matrix of the ideal storage ring; α, β, and γ are the Courant-Snyder functions; and ν_x is the horizontal tune.

Solving the above equation, one obtains

$$x_0 = \frac{1}{2\sin\pi\nu_x}\{[\sin\pi\nu_x + \alpha(s_0)\cos\pi\nu_x]A + \beta(s_0)\cos\pi\nu_x B\},$$

$$x_0' = \frac{1}{2\sin\pi\nu_x}\{-\gamma(s_0)\cos\pi\nu_x A + [\sin\pi\nu_x - \alpha(s_0)\cos\pi\nu_x]B\}. \qquad (A4)$$

The closed orbit at any other location s can be obtained by the transfer matrix, i.e.,

$$\begin{pmatrix} x(s) \\ x(s)' \end{pmatrix} = M(s|s_0)\begin{pmatrix} x(s_0) \\ x(s_0)' \end{pmatrix} = \frac{1}{2\sin \pi\nu_x} M_G \begin{pmatrix} A \\ B \end{pmatrix}, \tag{A5}$$

where M_G is the following matrix:

$$\begin{pmatrix} \sqrt{\frac{\beta(s)}{\beta(s_0)}}[\sin \hat{\psi}(s,s_0) + \alpha(s_0)\cos \hat{\psi}(s,s_0)] & \sqrt{\beta(s)\beta(s_0)}\cos \hat{\psi}(s,s_0) \\ -\frac{1+\alpha(s)\alpha(s_0)}{\sqrt{\beta(s)\beta(s_0)}}\cos \hat{\psi}(s,s_0) + \frac{\alpha(s_0)-\alpha(s)}{\sqrt{\beta(s)\beta(s_0)}}\sin \hat{\psi}(s,s_0) & \sqrt{\frac{\beta(s_0)}{\beta(s)}}[\sin \hat{\psi}(s,s_0) - \alpha(s)\cos \hat{\psi}(s,s_0)] \end{pmatrix},$$

and $\hat{\psi}(s,s_0) = \pi\nu_x - [\psi(s) - \psi(s_0)]$. Consequently, the closed-orbit change at location s is

$$x_{c.o.}(s) = \frac{1}{2\sin \pi\nu_x}\sqrt{\frac{\beta(s)}{\beta(s_0)}}[\sin \hat{\psi}(s,s_0) + \alpha(s_0)\cos \hat{\psi}(s,s_0)]A + \frac{1}{2\sin \pi\nu_x}\sqrt{\beta(s)\beta(s_0)}\cos \hat{\psi}(s,s_0)B. \tag{A6}$$

Substituting for $A = -D(s_0)\Delta p/p_0$ and $B = -D'(s_0)\Delta p/p_0$, one gets

$$\begin{aligned} x_{c.o.}(s) &= -\frac{\sqrt{\beta(s)}}{2\sin \pi\nu_x}\frac{1}{\sqrt{\beta(s_0)}}\{D(s_0)\sin \hat{\psi}(s,s_0) + [\alpha(s_0)D(s_0) \\ &\quad + \beta(s_0)D'(s_0)]\cos \hat{\psi}(s,s_0)\}\frac{\Delta p}{p_0} \\ &= -\frac{\sqrt{\beta(s)}}{2\sin \pi\nu_x}\sqrt{\mathcal{H}(s_0)}\cos \Psi(s,s_0)\frac{\Delta p}{p_0}, \end{aligned} \tag{A7}$$

which has the same form as Eq. (24) in Sec. III. The functions $\mathcal{H}(s_0)$ and $\Psi(s,s_0)$ are defined in Eqs. (17) and (22), respectively.

Similarly,

$$x'_{c.o.}(s) = \frac{\sqrt{\gamma(s)}}{2\sin \pi\nu_x}\sqrt{\mathcal{H}(s_0)}\cos[\hat{\psi}(s,s_0) - \chi(s_0) + \kappa(s)]\frac{\Delta p}{p_0}, \tag{A8}$$

where $\chi(s_0)$ and $\kappa(s)$ are defined in Eqs. (18) and (19).

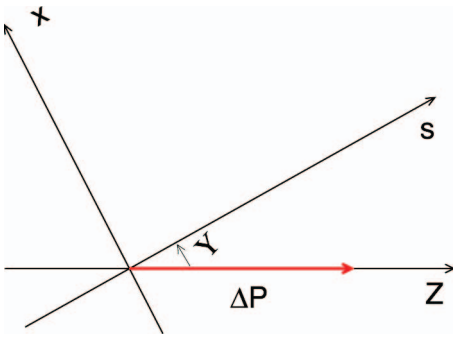

FIG. 9. (Color) The coordinate system in the rf cavity. The tilt angle between s and z is $\Upsilon = x'_{c.o.} = (D\delta + \zeta \sin \phi)'$.

For a ring accelerator, $x'_{c.o.}(s)$ can be expressed as

$$\begin{aligned} x'_{c.o.}(s) &= \frac{\sqrt{\gamma(s)}}{2\sin \pi\nu_x}\sum_{i=1}^{n}\sqrt{\mathcal{H}(s_i)}\cos[\hat{\psi}(s,s_i) - \chi(s_i) + \kappa(s)]\frac{\Delta p_i}{p_0} \\ &= -\frac{1}{\beta(s)}[\alpha(s)\zeta(s) + \xi(s)]\sin \phi_{rf}. \end{aligned} \tag{A9}$$

APPENDIX B: THE EQUILIBRIUM ANGLE

If the closed orbit has an angle with respect to the axis of the cavity, the particle will get a transverse kick when passing through. This is like the effect of a tilted cavity. The closed orbit is perturbed, and the particle will look for the equilibrium closed orbit. As is diagrammed in Fig. 9, the momentum changes in the rf cavity are

$$\Delta P_s = \Delta P_z \cos \Upsilon, \qquad \Delta P_x = -\Delta P_z \sin \Upsilon. \tag{B1}$$

Let the final closed orbit be

$$x_{c.o.} = x_{c.o,0} + D(s)\delta + \zeta(s)\sin \phi + x(s)_{ca}; \tag{B2}$$

then the angle Υ between the closed orbit and the cavity axis is

$$\Upsilon = D'(s_0)\delta + \zeta'(s_0)\sin \phi + x'(s_0)_{ca}. \tag{B3}$$

The transverse kick received from the cavity will be

$$\Delta x' = -[D'(s_0)\delta + \zeta'(s_0)\sin \phi + x'(s_0)_{ca}]\frac{\Delta p}{p_0}. \tag{B4}$$

Due to the above kick, the closed orbit angle change at the cavity location is given by

$$x'(s_0)_{ca} = \frac{1}{2\sin \pi\nu_x}[\sin \pi\nu_x - \alpha(s_0)\cos \pi\nu_x]\Delta x'. \tag{B5}$$

Solving the above equation, one gets the equilibrium angle at s_0,

$$x'(s_0)_{ca} = \frac{-R(s_0)[D'(s_0)\delta + \zeta'(s_0)\sin \phi]\Delta p/p_0}{2 + R(s_0)\Delta p/p_0}, \tag{B6}$$

where $R(s_0) = 1 - \alpha(s_0)\cot \pi\nu_x$. This is a second-order term because D', ζ', and $\Delta p/p_0$ are all small.

[1] M. C. Crowley-Milling and I. I. Rabinowitz, IEEE Trans. Nucl. Sci. **NS-18**, 1052 (1972).
[2] See, e.g., A. Piwinski, *CERN Accelerator School Proceedings*, CERN 87-03, p. 187.
[3] J. Feikes, K. Holldack, P. Kuske, and G. Wustefeld, *Proceedings of EPAC, 2004*, 2004, p. 1954.
[4] Y. Shoji, Phys. Rev. ST Accel. Beams **7**, 090703 (2004).
[5] H. Okamoto, Phys. Rev. E **50**, 4982 (1994).
[6] A. Piwinski and A. Wrulich DESY 76/07, Hamburg, 1976.
[7] A. W. Chao and A. Piwinski, DESY PET 77/07, Hamburg 1977.
[8] C. J. A. Corsten and H. L. Hagedoorn, Nucl. Instrum. Methods Phys. Res. **212**, 37 (1983).
[9] T. Suzuki, Part. Accel. **18**, 115 (1985).
[10] R. Baartman, TRIUMF Int. Rep, TRI-DN-89-K40, 1989.
[11] S. Y. Lee, Phys. Rev. E **49**, 5706 (1994).
[12] See, e.g., A. Chao and M. Tigner, *Handbook of Accelerator Physics and Engineering* (World Scientific, Singapore, 1998), p. 70.
[13] See, e.g., V. A. Yakubovich and V. M. Starzhinskii, *Linear Differential Equations with Periodic Coefficients* (Wiley, New York, 1975), Vol. 1, p. 76.
[14] See, e.g., S. Y. Lee, *Accelerator Physics* (World Scientific, Singapore, 1998), p. 210, Hamiltonian H1.
[15] M. Borland, "Elegant: A flexible SDDS-compliant code for accelerator simulation," Advanced Photon Source Light Source Note LS-287 (2000).
[16] D. Robin, E. Forest, C. Pellegrini, and A. Amiry, Phys. Rev. E **48**, 2149 (1993); D. Robin, H. Hama, A. Nadji, *Proc. Int. Conf. High Energy Accel*, 1956, p. 44.
[17] J. Feikes, K. Holldack, P. Kuske, and G. Wustefeld, ICFA Beam Dynamics Newsletters, No. 35, p. 82.
[18] Y. Shoji, S. Hisao, and T. Matsubara, *Proc. EPAC 2004*, 2004, p. 2356.